DOI 10.1007/s10593-017-2024-x

Chemistry of Heterocyclic Compounds **2017**, *53*(1), 78–86

Formation and characterization of mesoporous silica MCM-48 and polypyrrole composite

Monika Wysocka-Zolopa[1], Izabela Zablocka[1], Anna Basa[1], Krzysztof Winkler[1]*

[1] *Institute of Chemistry, University of Bialystok, Ciolkowskiego 1K, 15-245 Bialystok, Poland; e-mail: winkler@uwb.edu.pl*

Published in Khimiya Geterotsiklicheskikh Soedinenii, 2017, *53*(1), 78–86

Submitted September 30, 2016
Accepted November 9, 2016

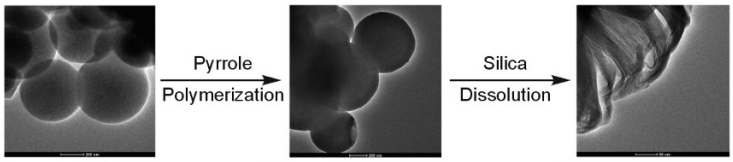

The composite of polypyrrole and mesoporous silica MCM-48, polypyrrole@MCM-48, was prepared. The silica nanopores were impregnated with dichloromethane solution of pyrrole by the capillary effect, and then monomer was polymerized inside the silica pores. The polymer was deposited on the walls of mesopores. Therefore, mesoporous structure was preserved in the composite. The structural features and physical properties of the composite were investigated by scanning and transmission electron microscopy, IR spectroscopy, thermogravimetry, and nitrogen adsorption/desorption. The polymer was extracted from the composite in form of long wires. The electrochemical properties of polypyrrole@MCM-48 composite and polypyrrole extracted from the composite were investigated. Both materials show stable electrochemical activity at positive potentials due to the polypyrrole oxidation. The electrochemical response of these polypyrrole wires is improved in comparison to the electrochemical behavior of polypyrrole incorporated into MCM-48 matrix.

Keywords: MCM-48, polypyrrole, electrochemical activity, mesoporous materials.

π-Conjugated polymers such as polypyrrole, polyaniline, polythiophene, and their derivatives have attracted considerable attention as electronic conductors. They exhibit unique properties, such as good electrical conductivity, as well as relatively good electrochemical and mechanical stability and catalytic activity. Various facile preparation methods have been reported to fabricate these macromolecular systems. Recent advances in the field of conducting polymers have focused on the formation of these materials at the nanolevel. The control of the size and morphology of such nanoparticles is very important for their practical potential application. Polymeric nanoparticles are very often incorporated into other materials to form composites.

Mesoporous silica molecular sieves can be used as a component of these composites.[1,2] Their pores are sufficiently large to allow fast diffusion of bulk molecules from the solution or from the gas phase. Mesoporous materials with monomers accommodated into the pores can serve as precursors for the polymerization process and composite formation. In the porous silica templates, tubular or fibrous conducting polymers are formed in the pores. Each pore in the template acts as a tiny reaction vessel of a precise diameter and length. The pores and channels of the mesoporous materials provide extensive control over the structure and size of the incorporated polymers and over the polymer–silica interaction.[3–6]

Mesoporous silicas MCM-48 and MCM-41 have attracted considerable attention for use as a host for polymeric particles because of their large surface area, ordered pore structure architecture, and narrow pore size distribution. The cubic MCM-48 contains two three-dimensional interwoven systems in a mirror-plane position relative to each other. MCM-41 exhibits a one-dimensional hexagonal bisectional pore system.[7] Recently, new procedures for forming MCM-48 small particles have been reported.[8–12] These procedures are based on modified Stober's synthesis of non-porous silica spheres.[13]

Conducting nanotubes or fibre polymers were prepared by *in situ* polymerization in silica particles using organic dopants. Most researchers have concentrated on mesoporous silica-supported nanocomposites containing polyaniline as a guest material.[14–20] Procedures for preparing mesoporous silica SBA-15 and polyaniline composites have been developed.[14–16] Silica was impregnated with the aniline monomer from the gas phase and then chemically oxidized to prepare the polyaniline@SBA-15 composite.[14] Mesoporous silica SBA-15 functionalized with *n*-propylaniline was used for *in situ* graft oxidative polymerization of aniline.[15] The polyaniline-grafted nanocomposite

material exhibited higher conductivity in comparison to non-grafted polyaniline/SBA-15 composite. A water impregnation method based on the electrostatic interaction between negatively charged mesopores and positive anilinium ions has been also proposed.[16] The gas-phase synthesis was used for the preparation of polyaniline@MCM-41 composites.[17,18] Polyaniline was deposited in the channels of silica to form 1D polymeric wires. These nanocomposite particles were adopted as a dispersed phase in electrorheological fluids.[17,18] Incorporation of polyaniline into 3D interconnected mesopores of silica KIT-6 *via* gas-phase method has been also performed.[19] Formed composite exhibits relatively good conductivity and can be used to monitor relative humidity of the environment. Silica mesoporous particles, MCM-41[21] and MCM-48,[22] were also used as components of composites in which polymeric material was deposited both on the surface of the silica particles and in the mesopores.

Mesoporous silica MCM-41 was used as host for self-assembly of monomer molecules inside the pores prior to polymerization into tubular poly(diphenylamine).[23] A confinement effect induced by mesoporous host MCM-41 on the electronic properties of nanotubular poly(diphenylamine) was reported. Poly(vinylacetate) was incorporated into the pores of MCM-48 and the structure of this composite was investigated.[6] In this case, the hydrophobic nature of the surface of the silica nanoparticles was increased by silylation with $-Si(CH_3)_3$ groups prior to polymerization. Poly[2,6-(4-phenylquinoline)] and other π-conjugated block polymers were incorporated into pores of silica from the liquid phase by capillary effect.[24] The size of pores determines the degree of aggregation of polymer chains within the pores. Polydiacetylene microsticks were formed in ordered hexagonal channels of silica from micellar structures of surfactant incorporated into the silica pores.[25] The MCM-41 functionalized with Cu(II) was used for oxidative polymerization of 1,4-diethynylbenzene into linearly aligned and highly conjugated polymer within the channels of silica.[26] Ni(II)-catalyzed polymerization of alkenes inside the silicate channels of MCM-41 affords polyyne@silica composite.[27]

Polypyrrole is one of the most promising conducting polymer because of its high conductivity, thermal, electrochemical, and environmental stabilities. A number of methods for preparation of this polymer have been reported in recent years, including electrochemical polymerization,[28–33] chemical polymerization,[33–42] and UV-induced polymerization.[43] These synthetic procedures are mainly focused on the formation of nanostructured polypyrrole materials. A simple and environmentally friendly, one-step oxidative polymerization method of fabrication of polypyrrole with fixed size and morphology using H_2O_2 as an oxidant was developed by Ramanavicius and coworkers.[34,35] Nanostructured conductive polypyrrole hydrogel was also formed using an interfacial polymerization method.[38] Such material exhibits good mechanical properties and excellent capacitance performance due to the three-dimensional porous nanostructure. The interfacial chemical polymerization at the interface of cyclohexane and water results in formation of highly-conducting and transparent polypyrrole sheets with a thickness ranging from nanometers to submicrons.[40] It was also reported that the nature of oxidant influences significantly structure, morphology, and electrochemical properties of chemically synthesized polypyrrole.[41] Electrochemical quartz crystal microbalance technique was used to evaluate mechanism of polypyrrole electropolymerization under pulse voltammetry conditions.[28] In general, electrochemically formed polypyrrole exhibits good capacitance properties and can be applied for construction of charge storage devices.[29–33]

Composites of polypyrrole and mesoporous silica particles were produced.[44–49] These studies were focused on the formation of 1D polymeric nanofibers within the ordered hexagonal arrays of silica MCM-41. Li and coworkers[44,45] obtained polypyrrole@MCM-41 composite by pyrrole vapor sorption within the pores followed by oxidative polymerization of the monomer. The same procedure was used for the formation of the polypyrrole@SBA-15 composites.[46] The rheological and dielectric properties of polypyrrole encapsulated in the pores of MCM-41 and SBA-15 are reflected in the increased interfacial polarizability of mesoporous silicate material and a higher electrorheological effect.[46,47] A sol-gel-based MCM-41 template polymerization of a pyrrole-containing diacetylic surfactant monomer succeeded in the formation of composites with a dense filling of silicate channels with the polymer.[48,49] Removing of silica from the composite results in the formation of long polymeric wires.[49] An interesting approach of polypyrrole deposition in the pores and on the surface of mesoporous silica was proposed by Choi and coworkers.[50] This method is based on the *in situ* generation of the NO^+ ions at the silica surface. The NO^+ ions selectively polymerize pyrrole on the silica surface to form uniform polymeric layer. Mesoporous silica nanoparticles were also incorporated into polypyrrole film under electrochemical conditions.[51]

This paper reports on the formation of a nanocomposite based on the MCM-48 silica and polypyrrole. The MCM-48 was chosen for these studies because of its special pore system providing effective mass transport,[7] particularly important in the electrochemical measurements. The synthesis was carried out in the liquid phase. The main goal of this study was to obtain a composite while preserving the mesoporous structure and depositing the polymer on the walls of the MCM-48 pores. The structure of the polypyrrole@MCM-48 composite was investigated. Special attention was paid to the electrochemical properties of the composite. Another goal of this study was to extract pure polymer wires from the composite and investigate their electrochemical properties.

Composites of MCM-48 and polypyrrole incorporated into pores of silica. The mesoporous silica MCM-48 was synthesized according to the procedure proposed by Schumacher et al.[8] The morphology of the synthesized material is shown in Figure 1*a*. The material takes the form of spherical particles, 400–800 nm in diameter. The size distribution of mesoporous MCM-48 particles is shown in the inset in Figure 1*a*. Transmission electron micrographs

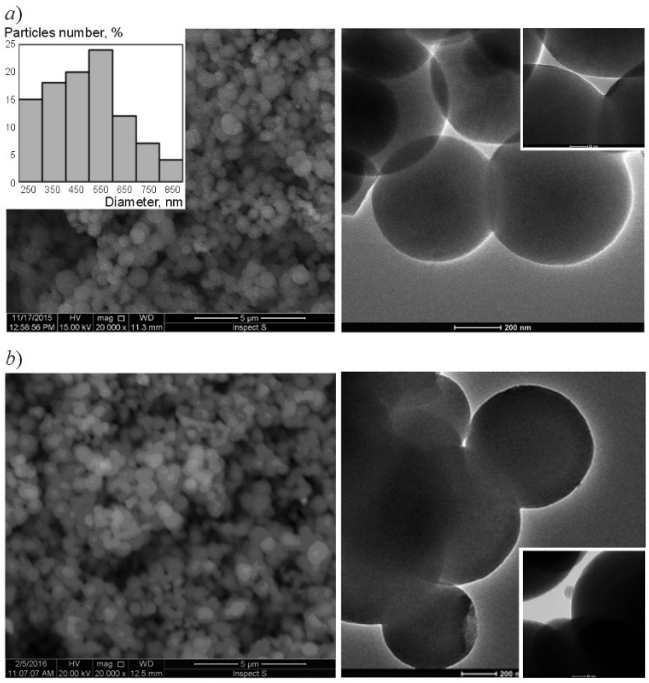

Figure 1. SEM (left panels) and TEM (right panels) images of *a*) MCM-48 and *b*) polypyrrole@MCM-48 composite. Inset in the SEM image of panel *a* shows size distribution of MCM-48 spherical particles.

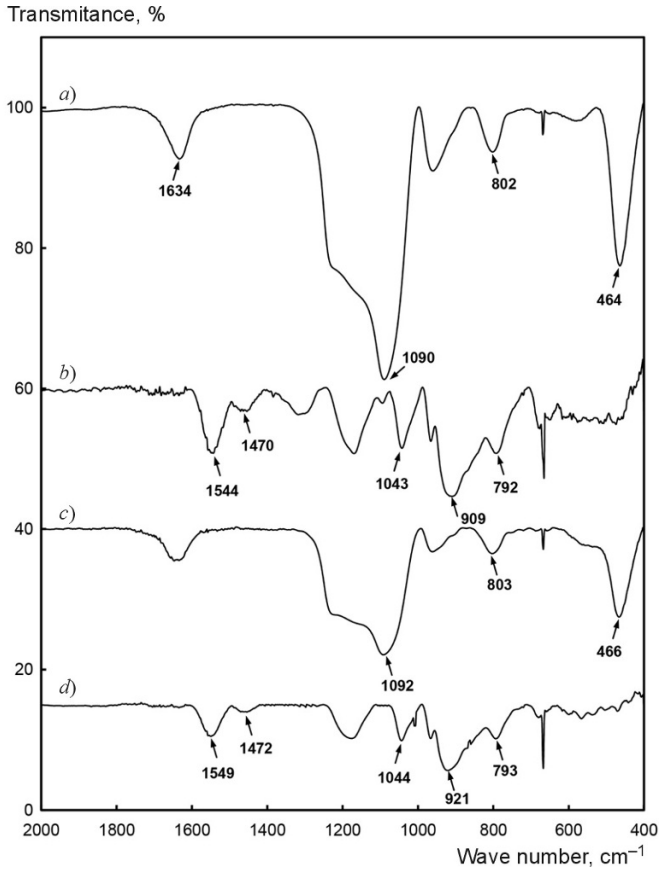

Figure 2. FTIR spectra of *a*) MCM-48, *b*) chemically prepared polypyrrole, *c*) polypyrrole@MCM-48 composite, and *d*) polypyrrole extracted from the pores of MCM-48 in KBr pallets.

provide visualization of the pore structure on the MCM-48 particle surface. The regular pore structure with pore diameter of about 3 nm is observed. The transmission Fourier transform infrared (FTIR) spectrum of MCM-48 is presented in Figure 2*a*. The strong band at 1090 cm^{-1} is related to the asymmetrical stretching vibrations of the Si–O–Si bonds. The signal at 802 cm^{-1} can be attributed to the symmetric stretching of the Si–O–Si bond. The signal related to the Si–O–Si bending mood is observed at 464 cm^{-1}. The band at about 1630 cm^{-1} is assigned to O–H bending vibrations of water molecules adsorbed at the silica surface.[52]

Polypyrrole was deposited in the mesopores of the MCM-48 host by pyrrole wetting due to the capillary effect followed by chemical polymerization. The color of the silica changes from white for pure MCM-48 to beige for the composite. Scanning electron microscopy (SEM) and transmission electron microscopy (TEM) images of the MCM-48 particles with the incorporated polypyrrole, polypyrrole@MCM-48, are shown in Figure 1*b*. Virtually no difference in the particle surface morphology of the pure MCM-48 host and polypyrrole@MCM-48 composite material was observed, which can serve as evidence of polypyrrole confinement within the MCM-48 channels, rather than surface adsorption and subsequent growth of the polymer. The regular pore structure is still visible. However, the morphology of walls of these pores differs from that observed for unmodified MCM-48. They exhibit much more irregular shape.

In Figures 2*b*,*c*, the IR spectra of polypyrrole and polypyrrole@MCM-48 in KBr are presented, respectively. In the case of pure polypyrrole, the characteristic bands of the polymer are consistent with those reported previously.[53–55] The bands at around 1544 and 1470 cm^{-1} can be assigned to the pyrrole ring fundamental vibrations. The bands that are observed in the 1000–1400 cm^{-1} range are very complex. The bands at around 1040 cm^{-1} correspond mostly to C–H in-plane bending and ring deformation. The broad band at about 910 cm^{-1} corresponds to the C–H and N–H ring out-of-plane bending. In the wave number range around 790 cm^{-1}, the bands responsible for the complex C=C stretch, C–C in-ring stretch, C–N stretch, C–C inter-ring stretch, C–N–C deformation, as well as C–H and N–H in-plane bending are observed. In the polypyrrole@MCM-48, the amount of polymer is relatively low. Therefore, the IR spectra of the polypyrrole@MCM-48 composite (Figure 2*c*) are predominated by the signals corresponding to the host silica. The bands related to polypyrrole are hidden in the large signal of MCM-48. To overcome these problems, the diffuse reflectance infrared Fourier transform (DRIFT) spectra of the chemically formed polypyrrole and polypyrrole@MCM-48 deposited on the surface of the SiC crystal were recorded. The relevant data are shown in Figure 3. In the wave number range below 1250 cm^{-1}, the spectrum is dominated by the large bands corresponding to the MCM-48 and SiC crystals. However, the bands for wave numbers higher than 1300 cm^{-1} indicate the presence of polypyrrole within the pores of MCM-48. These signals are much less intense

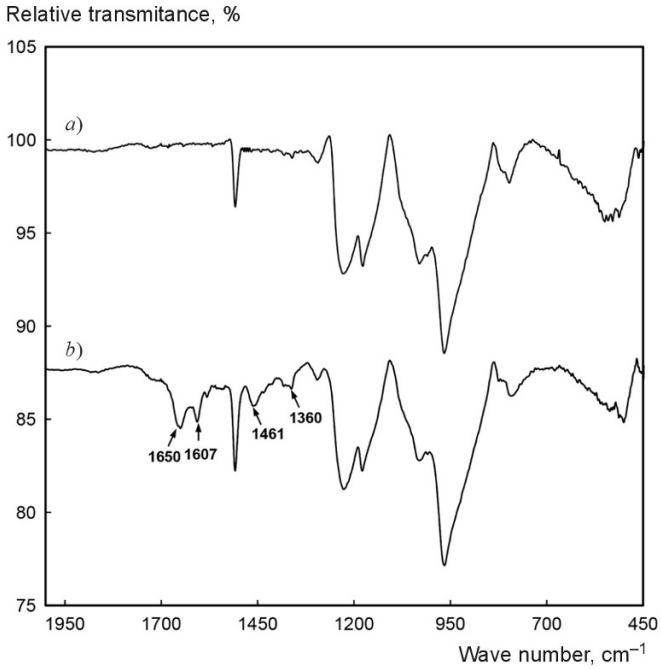

Figure 3. DRIFT spectra of *a*) MCM-48 and *b*) polypyrrole@MCM-48 composite with polypyrrole deposited at the surface of SiC crystal.

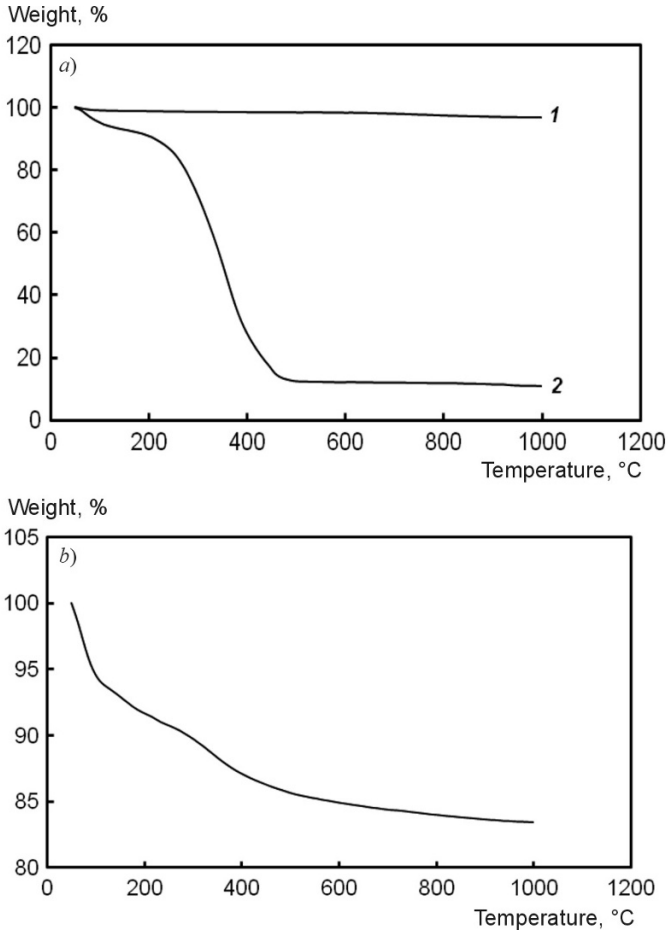

Figure 4. TGA curves of *a*) MCM-48 (curve *1*), pure chemically synthesized polypyrrole (curve *2*), and *b*) polypyrrole@MCM-48 composite.

than the bands of silica because of the presence of smaller amount of polypyrrole in the composite. The band assigned to the pyrrole ring fundamental vibrations is observed at around 1460 cm^{-1}. The absorption at 1607 cm^{-1} corresponds probably to the C=C ring stretching of pyrrole.[55] There is also number of bands related to polypyrrole presence in the wave number range from 1300 to 1400 cm^{-1} which are not observed for the pure MCM-48.

Figure 4 shows the results of a temperature gravimetric analysis (TGA) of the polypyrrole, MCM-48, and polypyrrole@MCM-48 samples. The silica particles are stable within the studied temperature range. Therefore, the residual weight percentage of the polypyrrole@MCM-48 sample refers to the weight percentage content of the silica in the composite. The thermal behavior of polypyrrole exhibits three weight-loss steps. The first weight loss below 100°C can be attributed to the loss of water. A slow decrease in the mass over the temperature range 100–250°C is related to the departure of the anionic dopant from the polymeric material. Polypyrrole is formed in its oxidized form and it is doped with Cl^- anions during the synthesis. The third weight loss, starting at around 250°C, is assigned to the decomposition of the polymeric material. The thermal stability of polypyrrole in the composite is higher than that of the pure polymeric material. The decomposition temperature of polypyrrole incorporated into the pores of MCM-48 is about 50°C higher than that of pure polypyrrole. The results of the TGA measurements enable the estimation of the polypyrrole amount present in the polypyrrole@MCM-48 composite. The mass loss at temperatures higher than 250°C, corresponding to the polymer decomposition, shows that the amount of polypyrrole within the composite does not exceed 5%.

The polymer product confined within the channels of the host silica was also confirmed by nitrogen sorption measurement. The N_2 adsorption-desorption isotherms and pore size distribution curves of the host MCM-48 and polypyrrole@MCM-48 composite are shown in Figure 5. The structural properties of these materials, obtained by nitrogen sorption measurements, are summarised in Table 1. Both samples show isotherms of type IV, suggesting that filling the MCM-48 pores with polypyrrole does not destroy the mesoporous structure of the host material. The incorporation of polypyrrole into the pores of MCM-48 results in a slight decrease in the average pore diameter from 3.1 nm for pure MCM-48 to 2.7 nm for the polypyrrole@MCM-48 composite. It has to be also noted a satisfactory agreement between the MCM-48 pore size obtained from nitrogen adsorption isotherm and from TEM

Table 1. Morphological parameters of the MCM-48 and polypyrrole@MCM-48 composite obtained by the nitrogen adsorption/desorption measurements

Material	BET surface, $m^2 \cdot g^{-1}$	Pore volume, $cm^3 \cdot g^{-1}$	Average pore diameter, nm
MCM-48	1520	0.74	3.1
Polypyrrole@MCM-48	1270	0.70	2.7

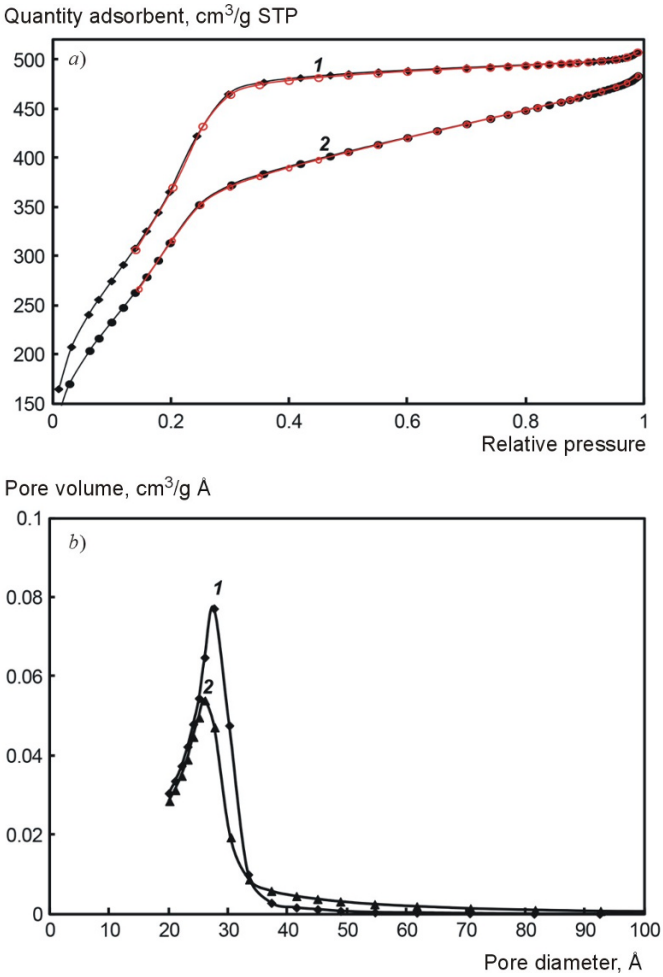

Figure 5. *a*) Nitrogen adsorption (black) / desorption (red) isotherms and *b*) pore size distribution for MCM-48 (curve *1*) and polypyrrole@ MCM-48 (curve *2*) composite.

images. These changes in the pore diameters correspond to changes in the pore volume from 0.74 to 0.70 $cm^3 \cdot g^{-1}$, respectively. Such small changes, both in the pore size and pore volume, indicate the partial filling of the MCM-48 pores with the polymer. A significant decrease in the BET specific surface area from 1520 to 1270 $m^2 \cdot g^{-1}$ was also observed after the incorporation of polypyrrole into the pores of MCM-48. Reductions in average pore diameter, pore volume, and surface area have been reported elsewhere after the incorporation of conducting polymers into particles of mesoporous silica.[6,14–19,26,44,46] However, changes of these parameters after polymer incorporation into the silica particles were much higher in comparison to values reported in this paper. In these composite materials, pores of the silica were almost completely filled with the dense polymeric phase.[48,49] Relatively small changes in the parameters listed in Table 1 for pure MCM-48 and the polypyrrole@MCM-48 composite indicate that the polymer is deposited at the surface of the silica pores rather than throughout the pores. Therefore, the mesoporous structure is preserved in the formed composite. The structure of the polypyrrole@MCM-48 composite is schematically presented in Figure 6.

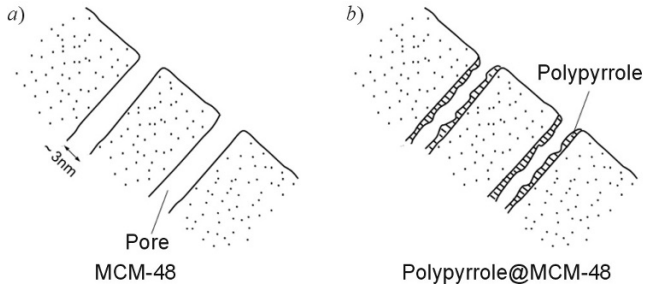

Figure 6. Schematic representation of *a*) the MCM-48 surface and *b*) MCM-48 surface with the pores filling with polypyrrole.

Polypyrrole extracted from the pores of MCM-48. In the next phase of the study, polypyrrole particles were extracted from the polypyrrole@MCM-48 composite. The composite was placed in a 2 M aqueous solution of NaOH for 10 min at 60°C. Under these conditions, the silica is dissolved.

The structure of polypyrrole extracted from the pores of silica MCM-48 was examined with SEM and TEM. The relevant data are shown in Figure 7. The images presented in this Figure clearly provide evidence for the nanotubular morphology of polypyrrole. The diameter of the long polypyrrole whiskers (around 1 nm) is lower in comparison with the diameter of the MCM-48 pores. The length of these polymeric nanowires ranges from 50 to 150 nm. The polypyrrole whiskers are aggregated into spherical structures (Fig. 7*a*), which resemble the shape, size, and mesoporous morphology of host MCM-48. However, they are very irregular and distorted due to the multiple washing and filtration steps. Further disintegration of these structures with high-energy ultrasound in aqueous suspension results in the formation of bundles of polypyrrole in which polypyrrole whiskers aggregate in parallel to each other after the removal of the solvent. The results of X-ray fluorescence spectroscopy (EDX) elemental analysis of polypyrrole extracted from the pores of MCM-48 show only signals corresponding to the carbon, nitrogen, and chlorine. These results indicate that silica MCM-48 was completely removed from the composite.

The FTIR spectra of polypyrrole nanowires (Fig. 2*d*) are very similar to the spectrum recorded for chemically polymerized pyrrole. This spectrum also shows that the MCM-48 silica host was completely removed from the

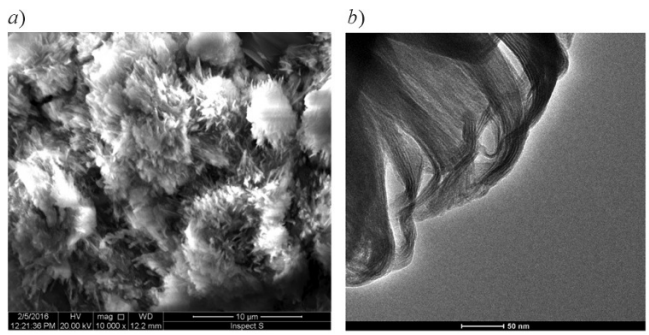

Figure 7. *a*) SEM and *b*) TEM images of polypyrrole extracted from the polypyrrole@MCM-48 composite.

composite. In the spectrum of the polypyrrole removed from the MCM-48 matrix, bands at around 1549 and 1472 cm^{-1}, assigned to the pyrrole ring fundamental vibrations, are observed. The bands at 1044 cm^{-1}, corresponding to C–H in-plane bending and ring deformation, as well as band at around 920 cm^{-1}, related to the C–H and N–H ring out-of-plane bending, are also observed. There is also a broad band at 793 cm^{-1} which is also present in the spectrum of pure pyrrole.

Electrochemical properties of polypyrrole@MCM-48 composite and polypyrrole extracted from composite. A large portion of the study focused on the electrochemical properties of the polypyrrole@MCM-48 composite and polypyrrole nanowires obtained after the host MCM-48 dissolution. The electrochemical properties of the polypyrrole depend on many factors such as the conditions of polymerization, dopant nature, morphology of the polymeric particles, and structure of polymeric film deposited at the electrode surface.[56–61] In Figure 8, the voltammetric behavior of a thin film of chemically produced polypyrrole and polypyrrole@MCM-48 composite are compared. In both cases, the material deposited at the electrode surface is electrochemically active at positive potentials due to polypyrrole oxidation. The Faradaic process is accompanied by anion transport from the solution to the solid phase. The pure, chemically produced polypyrrole exhibits very low electrochemical reversibility. A large capacitance current is observed on the voltammograms. The Faradaic currents of the polypyrrole oxidation (peak O_1) and reduction (peak R_1) are very low and overlap the capacitance current. This is typical of the behavior observed in aqueous solutions of chemically formed polypyrrole.[62,63]

Significant changes in the polymer redox processes were observed for the polypyrrole@MCM-48 composite compared to the pure polymer. In the composite, the polypyrrole oxidation potential shifts toward less negative potentials by about 100 mV. Peaks related to the oxidation and reduction of the polymeric phase are more pronounced, relative to those of the pure polymer. It is also observed that, within the potential range of the polypyrrole oxidation current, separated peaks are observed (indicated by arrows in Fig. 8*b*). The oxidation of polypyrrole occurs in the pores of the MCM-48 particles. The different sizes of the pores and different degree of filling of these pores with polypyrrole are responsible for the observation of multiple peaks in the potential range of polypyrrole oxidation. For a sweep rate range of 10–100 $mV \cdot s^{-1}$, a linear relationship between the polypyrrole oxidation peak current and the sweep rate is observed, indicating the electrode processes involving surface-confined electroactive materials.

The voltammetric behavior of the polypyrrole extracted from the pores of silica MCM-48 is presented in Fig. 9. A very significant improvement in the electrochemical reversibility of this material, in comparison to the electrode processes of the chemically produced polypyrrole and polypyrrole@MCM-48 composite, is observed. The potential separation between the polymer oxidation and reduction processes also decreases. The dependence of the voltammetric behavior on the sweep rate was also

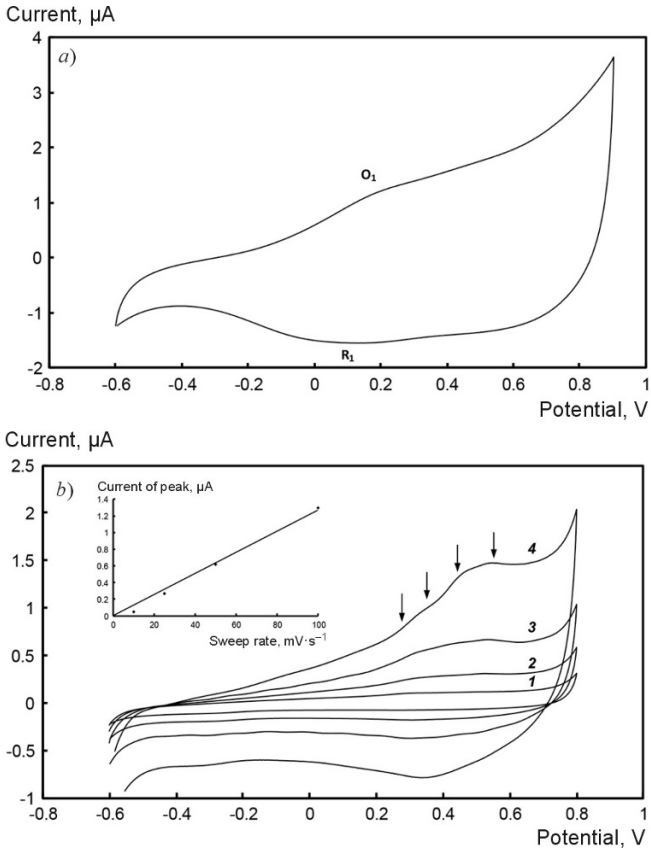

Figure 8. Cyclic voltammograms recorded for Au electrode (diameter 1.5 mm) covered with *a*) chemically synthesized polypyrrole and *b*) polypyrrole@MCM-48 composite in water containing 0.1 M NaCl. The sweep rate was 10 $mV \cdot s^{-1}$ (curve *1*), 25 $mV \cdot s^{-1}$ (curve *2*), 50 $mV \cdot s^{-1}$ (curve *3*), 100 $mV \cdot s^{-1}$ (curve *4*). The inset in panel *b* shows dependence of the polypyrrole oxidation peak current on the sweep rate.

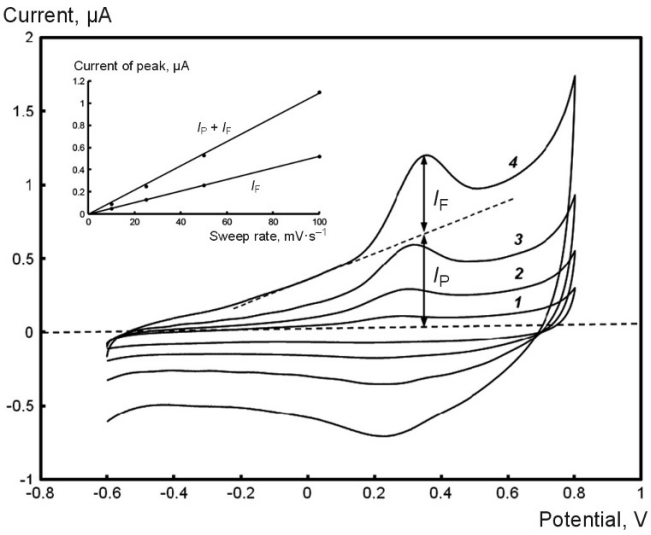

Figure 9. Cyclic voltammograms recorded for Au electrode (diameter 1.5 mm) covered with polypyrrole whiskers extracted from the polypyrrole@MCM-48 composite in water containing 0.1 M NaCl. The sweep rate was 10 $mV \cdot s^{-1}$ (curve *1*), 25 $mV \cdot s^{-1}$ (curve *2*), 50 $mV \cdot s^{-1}$ (curve *3*), 100 $mV \cdot s^{-1}$ (curve *4*). The inset shows dependence of the Faradaic component and total polypyrrole oxidation peak current on the sweep rate.

investigated for the electrode coated with a film of polypyrrole wires. Both the Faradaic and capacitance components of the polypyrrole oxidation process are linearly dependent on the sweep rate, in the same way as the behavior observed for an electrode coated with the polypyrrole@MCM-48 composite. The improvement in the electrochemical properties of the polypyrrole wires, particularly in comparison with the voltammetric behavior of chemically produced bulk materials (Fig. 8*a*), is related to the structure of the polypyrrole particles. Film formed from long and thin needles of polypyrrole is more porous. The real surface of such material is also very large. These two factors are responsible for the observed improvement in the electrochemical properties of polypyrrole extracted from the pores of silica MCM-48.

A composite consisting of mesoporous silica MCM-48 and conductive polypyrrole confined within the channels of MCM-48 was synthesized by wet impregnation of the host material with a solution containing pyrrole, followed by chemical polymerization within the pores. The insertion of polypyrrole was confirmed by the N_2 adsorption measurements, IR spectroscopy, and thermogravimetry. The amount of polymer deposited on the silica was relatively low, at about 5%. The polypyrrole was deposited inside the pores on their walls. Therefore, the mesoporous structure of the host material was preserved. Polypyrrole was frequently used for inorganic, organic, and biologically active compounds sensing.[64–70] Composite of polypyrrole and MCM-48 can be also used for sensor construction. The significant enhancement of analytical signal should be expected because of high surface area of polypyrrole deposited inside of MCM-48 pores.

The polypyrrole can be removed from the MCM-48 matrix by silica dissolution in an aqueous solution of NaOH. The polypyrrole forms spherical structures consisting of thin and long whiskers of the polymer. Both the whiskers of polypyrrole and polypyrrole incorporated into the pores of MCM-48 exhibit electrochemical activity due to polymer oxidation and the doping of the solid phase with anions from the solution. The electrochemical response of the polypyrrole extracted from the composite is superior to that of chemically synthesized bulk material and the polymer incorporated into a silica matrix. Such an improvement in the electrochemical properties of polypyrrole is particularly important for further practical application of this polymer in charge-storage and energy-conversion devices.

Experimental

Chemicals. The supporting electrolyte NaCl was used as received from Aldrich Chemical Co. Pyrrole and $FeCl_3$ were used as received from Aldrich Inc. The *n*-hexadecyltrimethylammonium bromide template, tetraethyl orthosilicate, aqueous ammonia, and ethanol were used as received from Aldrich Chemical Co. These were used for the synthesis of MCM-48 spheres. Pure deionized water with a resistivity of 18.2 MΩ·cm was obtained from a Milli-Q/Millipore system.

Instrumentation. Voltammetric experiments were performed using a potentiostat/galvanostat Model 283 (EG&G Instruments) with a three-electrode cell. An AUTOLAB system was controlled with the GPES 4.9 software of the same manufacturer. A gold disc with a diameter of 1.5 mm (Bioanalytical Systems, Inc.) was used as the working electrode. Prior to the start of the experiment, the electrode was polished with a fine carborundum paper and then with a 0.5-μm alumina slurry. Subsequently, the electrode was sonicated in water to remove traces of alumina from the gold surface, washed with water, and then dried. An Ag/AgCl-saturated KCl electrode was used as the reference electrode. The reference electrode was separated from the working electrode by a ceramic tip (Bioanalytical Systems Inc.). The counter electrode was a platinum tab with an area of about 0.5 cm^2.

The morphology of the obtained materials was secondary-electron imaged using an Inspect S50 scanning-electron microscope (FEI Company, Hillsboro, Oregon, USA). The accelerating voltage of the electron beam was either 20 or 25 keV and the average working distance was 10 mm. TEM images were obtained using a Tecnai G^2 20 X-TWIN microscope (FEI Company, Hillsboro, Oregon, USA) with an LaB6 emitter and an HAADF detector operating at 120/200 kV. For energy dispersive X-ray fluorescence measurements, an EDX instrument and software of Ametek (Berwyn, Pennsylvania, USA) were used. This software facilitates standardless quantification of atomic weight and atomic percentage. The accelerating voltage for the electron beam was 20 keV, and the working distance was 10 mm. The FT-IR spectra were recorded using a Magna IR 550 Series II spectrometer with a spectral resolution of 4 cm^{-1}.

Thermogravimetric analysis (TGA) was performed using a Mettler Toledo Star TGA/DSC system. Nitrogen was used as the purge gas (0.1 $dm^3 \cdot min^{-1}$). Samples weighing 2 mg were placed in aluminum pans and heated from 50 to 1000°C at a heating rate of 10°C min^{-1}. Nitrogen adsorption/desorption isotherms were recorded at 77.15 K with a Micrometrics ASAP 2020 automatic sorption analyzer.

Synthesis procedures. MCM-48 was produced according to procedure proposed by Schumacher et al.[8] A template, *n*-hexadecyltrimethylammonium bromide, was dissolved in a H_2O–EtOH mixture. Aqueous ammonia was added to the surfactant solution. The solution was then stirred for 10 min. Next, tetraethoxysilane was added. The molar composition of the gel was 1 mol tetraethoxysilane / 12.5 mol NH_3 / 54 mol EtOH / 0.4 mol template / 174 mol H_2O. After 2 h of stirring at room temperature, the formed solid was filtrated, washed with distilled water, and then dried in air. The template was removed by calcination at 550°C for 6 h.

To obtain the polypyrrole@MCM-48 composite, silica particles were placed in 1,2-dichloromethane containing 1 $mol \cdot dm^{-3}$ pyrrole for 2 h. Next, MCM-48 particles with incorporated polypyrrole were filtered and washed in water a few times to remove the pyrrole from the MCM-48 particle surface. Pyrrole accumulated in the pores of the MCM-48 was polymerized in an aqueous solution containing $FeCl_3$ for 2 h. The mass ratio of $FeCl_3$ to MCM-48 was 13:1. The formed polypyrrole@MCM-48 composite

was filtered, washed with water, and then dried at 50°C in air.

To extract the polypyrrole wires from the polypyrrole@MCM-48 composite, silica particles with polypyrrole filling the pores were placed in 2 M aqueous solution of NaOH at 60°C for 10 min. Under these conditions, the silica was dissolved. The remaining polypyrrole was filtered and washed with water a few times. This procedure was repeated four times. Finally, the polypyrrole extracted from the composite was dried at 80°C for 12 h under a nitrogen atmosphere.

Electrochemical measurements. In the electrochemical measurements, the synthesized materials were deposited at the electrode surface by a drop-coating method. A certain amount of composite material was dispersed in dichloromethane by sonication. The amount of the composite dispersed in the dichloromethane varied, depending on the desired thickness of the solid layer. Typically, a 5 μl drop of solution was applied to the electrode surface and heated to dry it before the addition of subsequent drops to form a coat of the desired thickness. The thickness of the film deposited at the surface of the gold electrode was determined with scanning electron microscopy.

The electrochemical properties of the composite film were studied in water containing only the supporting electrolyte. In this case, the electrode covered with the film was rinsed several times with dichloromethane and water, and then placed in a solution containing the supporting electrolyte. The modified electrode was allowed to equilibrate for 10 min while degassing with argon in a fresh solution before electrochemical measurements were performed.

The authors thank Dr. Alina Dubis for her assistance with the IR measurements and Olena Mykhailiv for her assistance with the nitrogen adsorption/desorption analysis.

References

1. Run, M. T.; Wu, S. Z.; Zhang, D. Y.; Wu, G. *Mater. Chem. Phys*. **2007**, *105*, 341.
2. Wei, L.; Hu, N.; Zhang, Y. *Materials* **2010**, *3*, 4066.
3. Frisch, H. L.; Mark, J. E. *Chem. Mater*. **1996**, *8*, 1735.
4. Frisch, H. L.; Maaref, S.; Xue, Y.; Beaucage, G.; Pu, Z.; Mark, J. E. *J. Polym. Sci.*, *Part A: Polym. Chem.* **1996**, *34*, 673.
5. Moller, K.; Bein, T.; Fischer, R. X. *Chem. Mater*. **1998**, *10*, 1841.
6. He, J.; Shen, Y.; Yang, J.; Evans, D. G.; Duan, X. *Chem. Mater*. **2003**, *15*, 3894.
7. Wei, F.; Yang, J.; Gu, F. N.; Gao, L.; Zhu, J. H. *Microporous Mesoporous Mater.* **2010**, *130*, 266.
8. Schumacher, K.; Grün, M.; Unger, K. K. *Microporous Mesoporous Mater.* **1999**, *27*, 201.
9. Schumacher, K.; Ravikovitch, P. I.; Du Chesne, A.; Neimark, A. V.; Unger, K. K. *Langmuir* **2000**, *16*, 4648.
10. Lind, A.; von Hohenesche, C. F.; Smått, J.-H.; Lindén, M.; Unger, K. K. *Microporous Mesoporous Mater.* **2003**, *66*, 219.
11. Nakamura, T.; Yamada, H.; Yamada, Y.; Gürtanyel, A.; Hartmann, S.; Hüsing, N.; Yano, K. *Langmuir* **2010**, *26*, 2002.
12. Kim, T.-W.; Chung, P.-W.; Lin, V. S.-Y. *Chem. Mater*. **2010**, *22*, 5093.
13. Stöber, W.; Fink, A.; Bohn, E. *J. Colloid Interface Sci*. **1968**, *26*, 62.
14. Cho, M. S.; Choi, H. J.; Kim, K. Y.; Ahn, W. S. *Macromol. Rapid Commun.* **2002**, *23*, 713.
15. Sasidharan, M.; Mal, N. K.; Bhaumik, A. *J. Mater. Chem*. **2007**, *17*, 278.
16. Weng, S.; Lin, Z.; Zhang, Y.; Chen, L.; Zhou, J. *React. Funct. Polym*. **2009**, *69*, 130.
17. Cho, M. S.; Choi, H. J.; Ahn, W.-S. *Langmuir* **2004**, *20*, 202.
18. Fang, F. F.; Choi, H. J.; Ahn, W. S. *Compos. Sci. Technol*. **2009**, *69*, 2088.
19. Dou, Y.-Q.; Zhai, Y.; Zeng, F.; Liu, X.-X.; Tu, B.; Zhao, D. *J. Colloid Interface Sci*. **2010**, *341*, 353.
20. Takei, T.; Yoshimura, K.; Yonesaki, Y.; Kumada, N.; Kinomura, N. *J. Porous Mater*. **2005**, *12*, 337.
21. Feng, X.; Yang, G.; Liu, Y.; Hou, W.; Zhu, J.-J. *J. Appl. Polym. Sci*. **2006**, *101*, 2088.
22. Sun, X.; Ren, J.; Zhang, L. W.; Chen, L.; Li, H.; Li, R.; Ma, J. T. *Synth. Met*. **2010**, *160*, 2244.
23. Lee, K.-P.; Showkat, A. M.; Gopalan, A. I.; Kim, S.-H.; Choi, S.-H. *Macromolecules* **2005**, *38*, 364.
24. Ho, S. W.; Kwei, T. K.; Výprachtický, D.; Okamoto, Y. *Macromolecules* **2003**, 36, 6894.
25. Aida, T.; Tajima, K. *Angew. Chem.*, *Int. Ed*. **2001**, *40*, 3803.
26. Lin, V. S.-Y.; Radu, D. R.; Han, M.-K.; Deng, W.; Kuroki, S.; Shanks, B. H.; Pruski, M. *J. Am. Chem. Soc*. **2002**, *124*, 9040.
27. Cardin, D. J.; Constantine, S. P.; Gilbert, A.; Lay, A. K.; Alvaro, M.; Galletero, M. S.; Garcia, H.; Marquez, F. *J. Am. Chem. Soc*. **2001**, *123*, 3141.
28. Plausinaitis, D.; Ratautaite, V.; Mikoliunaite, L.; Sinkevicius, L.; Ramanaviciene, A.; Ramanavicius, A. *Langmuir* **2015**, *31*, 3186.
29. Wolfart, F.; Dubal, D. P.; Vidotti, M.; Holze, R.; Gómez-Romero, P. *J. Solid State Electrochem.* **2016**, *20*, 901.
30. Li, K.; Zhang, H.; Tang, T.; Tang, Y.; Wang, Y.; Jia, J. *J. Power Sources* **2016**, *324*, 368.
31. Warren, R.; Sammoura, F.; Teh, K. S.; Kozinda, A.; Zang, X.; Lin, L. *Sens. Actuators*, *A* **2015**, *A231*, 65.
32. Wysocka-Żołopa, M.; Winkler, K. *J. Power Sources* **2015**, *300*, 472.
33. Chen, S.; Zhitomirsky, I. *Mater. Lett*. **2014**, *125*, 92.
34. Leonavicius, K.; Ramanaviciene, A.; Ramanavicius, A. *Langmuir* **2011**, *27*, 10970.
35. Kausaite-Minkstimiene, A.; Mazeiko, V.; Ramanaviciene, A.; Ramanavicius, A. *Colloids Surf.*, *A* **2015**, *483*, 224.
36. Ghamouss, F.; Brugère, A.; Anbalagan, A. C.; Schmaltz, B.; Luais, E.; Tran-Van, F. *Synth. Met.* **2013**, *168*, 9.
37. Qiao, Y.; Shen, L.; Wu, M.; Guo, Y.; Meng, S. *Mater. Lett*. **2014**, *126*, 185.
38. Shi, Y.; Pan, L.; Liu, B.; Wang, Y.; Cui, Y.; Bao, Z.; Yu, G. *J. Mater. Chem. A* **2014**, *2*, 6086.
39. Malhotra, U.; Maity, S.; Chatterjee, A. *J. Appl. Polym. Sci.* **2015**, *132*, 41336.
40. Qi, G.; Wu, Z.; Wang, H. *J. Mater. Chem. C* **2013**, *1*, 7102.
41. Shinde, S. S.; Gund, G. S.; Dubal, D. P.; Jambure, S. B.; Lokhande, C. D. *Electrochim. Acta* **2014**, *119*, 1.
42. Shinde, S. S.; Gund, G. S.; Kumbhar, V. S.; Patil, B. H.; Lokhande, C. D. *Eur. Polym. J*. **2013**, *49*, 3734.
43. Ramanavicius, A.; Karabanovas, V.; Ramanaviciene, A.; Rotomskis, R. *J. Nanosci. Nanotechnol*. **2009**, *9*, 1909.
44. Cheng, Q.; Pavlinek, V.; Li, C.; Lengalova, A.; He, Y.; Saha, P. *Mater. Chem. Phys*. **2006**, *98*, 504.
45. Cheng, Q.; He, Y.; Pavlinek, V.; Lengalova, A.; Li, C.; Saha, P. *J. Mater. Sci*. **2006**, *41*, 5047.
46. Cheng, Q.; Pavlinek, V.; Lengalova, A.; Li, C.; He, Y.; Saha, P. *Microporous Mesoporous Mater.* **2006**, *93*, 263.
47. Cheng, Q.; Pavlinek, V.; Lengalova, A.; Li, C.; Belza, T.; Saha, P. *Microporous Mesoporous Mater.* **2006**, *94*, 193.

48. Ikegame, M.; Tajima, K.; Aida, T. *Angew. Chem.*, *Int. Ed*. **2003**, *42*, 2154.
49. Guo, R.; Li, G.; Zhang, W.; Shen, G.; Shen, D. *ChemPhysChem* **2005**, *6*, 2025.
50. Jung, Y.; Spray, R. L.; Kim, J. H.; Kim, J. M.; Choi, K.-S. *Chem. Commun*. **2010**, *46*, 6566.
51. Nakayama, M.; Yano, J.; Nakaoka, K.; Ogura, K. *Synth. Met.* **2002**, *128*, 57.
52. Alba, M. D.; Luan, Z.; Klinowski, J. *J. Phys. Chem.* **1996**, *100*, 2178.
53. Mathys, G. I.; Truong, V.-T. *Synth. Met.* **1997**, *89*, 103.
54. Lei, J.; Liang, W.; Martin, C. R. *Synth. Met.* **1992**, *48*, 301.
55. Kostić, R.; Raković, D.; Stepanyan, S. A.; Davidova, I. E.; Gribov, L. A. *J. Chem. Phys*. **1995**, *102*, 3104.
56. Omastová, M.; Trchová, M.; Kovářová, J.; Stejskal, J. *Synth. Met.* **2003**, *138*, 447.
57. Otero, T. F.; Cantero, I.; Grande, H. *Electrochim. Acta* **1999**, *44*, 2053.
58. Patois, T.; Lakard, B.; Monney, S.; Roizard, X.; Fievet, P. *Synth. Met.* **2011**, *161*, 2498.
59. Silk, T.; Hong, Q.; Tamm, J.; Compton, R. G. *Synth. Met.* **1998**, *93*, 59.
60. Nishio, K.; Fujimoto, M.; Ando, O.; Ono, H.; Murayama, T. *J. Appl. Electrochem*. **1996**, *26*, 425.
61. Kupila, E.-L.; Kankare, J. *Synth. Met.* **1995**, *74*, 241.
62. Lee, H. S.; Hong, J. *Synth. Met*. **2000**, *113*, 115.
63. Dubal, D. P.; Patil, S. V.; Jagadale, A. D.; Lokhande, C. D. *J. Alloys Compd*. **2011**, *509*, 8183.
64. Hsueh, C.; Brajter-Toth, A. *Anal. Chem*. **1994**, *66*, 2458.
65. Okuno, H.; Kitano, T.; Yakabe, H.; Kishimoto, M.; Deore, B. A.; Siigi, H.; Nagaoka, T. *Anal. Chem.* **2002**, *74*, 4184.
66. Shahrokhian, S.; Zare-Mehrjardi, H. R. *Electroanalysis* **2009**, *21*, 157.
67. Ayenimo, J. G.; Adeloju, S. B. *Talanta* **2016**, *148*, 502.
68. Oukil, D.; Benhaddad, L.; Aitout, R.; Makhloufi, L.; Pillier, F.; Saidani, B. *Sens. Actuators*, *B* **2014**, *B204*, 203.
69. Ansari, R.; Delavar, A. F.; Mohammad-khah, A. *Microchim. Acta* **2012**, *178*, 71.
70. Tavoli, F.; Alizadeh, N. *Sens. Actuators*, *B* **2013**, *B176*, 761.